CIRP Annals - Manufacturing Technology 71 (2022) 153–156

Contents lists available at ScienceDirect

CIRP Annals - Manufacturing Technology

journal homepage: https://www.editorialmanager.com/CIRP/default.aspx

Electrochemical additive manufacturing of NiCoFeCuMo high entropy alloys using a combined dissolution-deposition system

M. Sundaram[a,*], A. Brant[a], K. Rajurkar (1)[b]

[a] Department of Mechanical and Materials Engineering, University of Cincinnati, Cincinnati, OH, USA
[b] Department of Mechanical and Materials Engineering, University of Nebraska-Lincoln, Lincoln, NE, USA

ARTICLE INFO

Article history:
Available online 8 April 2022

Keywords:
Additive manufacturing
Process control
Compositional grading

ABSTRACT

Compositionally-graded NiCoFeCuMo high-entropy-alloy parts were fabricated using electrochemical additive manufacturing operated in a combined dissolution-deposition manner. Dynamic solution concentration control and compositional grading were achieved using concurrent dissolution of source metal anodes. A common supporting bath to accommodate dissolution and deposition of all metals was identified by separately studying dissolution processes and selecting ionic influences on deposition. Results from the combined system showed that Ni and Mo contents could be graded the most controllably, followed by Co and Fe, and finally Cu. Output atomic percentages ranged from 3-48%, with some regions meeting the 5-35% definition of a high entropy alloy.

1. Introduction

High-entropy alloys (HEAs) contain multiple principal elements in equimolar or near-equimolar ratios [1], at atomic ratios between 5 and 35%, presenting countless new compositional and combinations beyond those of conventional alloys. Novel material property combinations (ie: mechanical, thermal, and magnetic) can occur within a single HEA [2]. Such materials can serve as solutions to advanced engineering problems; for example, a wear- and radiation-resistant replacement to Co-based coatings in nuclear installations [3].

However, conventional bulk and additive manufacturing of HEAs is rife with obstacles in compositional, structural, and property control; primarily due to the thermal nature of the underlying processes. Major challenges include solute partitioning upon solidification during casting; or undesired structural, property, or contamination changes upon powder sintering [2]. The complex, localized laser-scanning occurring in conventional AM further exacerbates these obstacles, including poor surface quality, internal defects, thermal stresses and cracks, porosity, and inconsistency in output geometry and properties [4]. For powder-based AM, elemental powder availability presents a challenge [5]. When the metals within an alloy possess increasingly-dissimilar thermal or optical properties, their processing becomes increasingly complex [6]; this presents: difficulty predicting and achieving target phases and microstructures [3] due to a highly-complex material response to thermal input [5], increased challenges in process and path planning [7]. Highly-unpredictable and nonlinear processes, characterized by increased statistical fluctuations and chaos, require significant additional work in the assessment and management of process performance metrics. This negatively impacts the fulfillment of quality, cost, time, and customization demands in industrial adoption [8].

The metallurgical and logistical challenges can be overcome using electrochemical additive manufacturing (ECAM), an emerging, non-traditional AM process performed using localized electrochemical deposition at room temperature [9]. Prior ECAM demonstrations across material systems include single metals [10], binary alloys such as NiCu [11], and a quaternary NiCoFeCu alloy [12]. Deposition profile predictions have been demonstrated using electrochemical simulation [13]. However, prior studies used pre-mixed, fixed-composition plating baths that yielded a limited degree of compositional control, even under a locally-varied deposition signal [12]

This study aims to further expand the capabilities of ECAM by (1) identifying the necessary electrochemical conditions to achieve *separate* dissolution and deposition of five alloying elements, reaching the domain of HEAs, with each metal sourced into the solution by the dissolution of its corresponding solid-state anode and (2) fine-tuning the conditions found for the separate processes to a single set of conditions, to demonstrate successful dissolution-deposition within a unified system in which ionic concentrations are dynamically sourced by sacrificial anodic dissolution, yielding compositionally-graded deposits of the five-metal alloy.

2. Methods

This study initially set out to address the challenge of identifying suitable electrochemical conditions to operate the combined dissolution-deposition of HEAs by ECAM. The NiCoFeCuMo HEA was chosen as the material system to undergo processing [14]. The expected co-deposition relationships among the metal cations [15] are illustrated in Fig. 1(a). Common supporting species for plating these metals, and their roles in the metal deposition process, are illustrated in Fig. 1(b).

* Corresponding author at: University of Cincinnati, Mechanical and Materials Engineering, 2851 Woodside Dr, Cincinnati, OH 45221-0072, United States.
E-mail address: murali.sundaram@uc.edu (M. Sundaram).

https://doi.org/10.1016/j.cirp.2022.03.009
0007-8506/

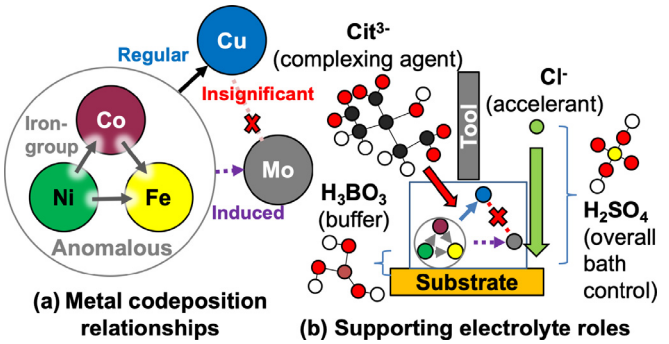

Fig. 1. Summary of solution species behaviors.

Dissolution and deposition – even for a single metal – are separate physical processes; the successful operation of either one requires distinct electrochemical conditions, which must be balanced to perform both in a single electrolytic environment. Fabrication of the NiCoFeCuMo HEA part using ECAM requires an electrochemical environment that is further fine-tuned to handle both processes for all five constituent species at once. In this study, an operable range of electrochemical conditions was initially identified by performing dissolution and deposition in separate stages with deliberate, incremental variations from a reference starting bath concentration. The essential requirements for the dissolution of each separate metal were first identified. The dissolved separate-metal baths were then mixed into plating baths, with concentrations of supporting species and metal cations varied across separate trials. The resulting five-metal deposition under the influence of varying bath composition was observed. All electrochemical processes were controlled using a custom, in-house-built system operated by an Arduino Mega 2560, shown in Fig. 2(a). The dissolution and deposition experiments were performed in separate chambers of a multi-chamber electrochemical cell, shown in Fig. 2(b).

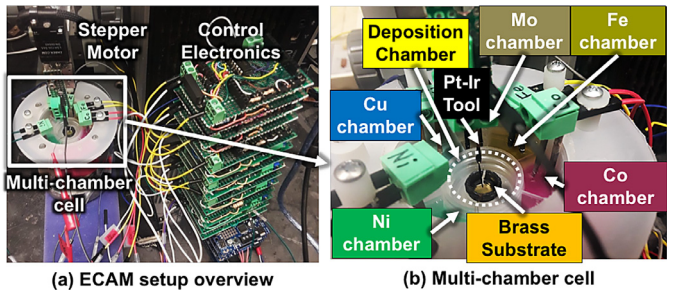

Fig. 2. ECAM dissolution-deposition setup: (a) overview, (b) cell.

Dissolution of each species j – Ni, Co, Fe, Cu, or Mo – was performed in separate volumes of 1, 1, 1, .5, and .5 mL to target concentrations c_{tj} of: .4, .1, .02, .02, and .02 M. A .05 M Mo solution was also prepared. The channel for each metal, illustrated in Fig. 3(a), consisted of a 2-electrode cell controlled by a voltage-application and current-monitoring circuit. The dissolution current $i_j(t)$ was sampled at regular 1 s timesteps Δt, contributing charge $q_j(t)=i_j(t)\Delta t$. Series resistors R_{series} (68, 300, 68, 51, and 68 Ω) were included to avoid saturation of current readings beyond the hardware limits. Based on Faraday's Law – using dissolved moles $n_j(t)$, chamber volume V_j, species valence z_j, (+2, +2, +3, +2, or +6) and Faraday's constant F (96485 C/mol) – the accumulated concentration up to time t was calculated as $c_j(t)=\Sigma[q_j(t)/(z_jFV_j)]$. Upon $c_j(t)$ reaching c_{tj}, the channel was relay-switched from active to inactive (open-circuit) state, and both electrodes were manually removed. The exact current efficiencies and geometries of the cells were not accounted for; concentrations are therefore approximate values. Given a starting bath (.485 M H_3BO_3, .00018 M H_2SO_4, .07 M Na_3Cit, and .1 M NaCl); Fe and Mo dissolved without complication, while the remaining metals formed undesired anodic precipitates. Select variations in the blank baths were therefore tested to identify the necessary variations for Ni, Co, and Cu dissolution. An overview of all blank bath combinations is provided in Table 1.

Table 1
Blank baths (all contain .485 M H3BO3).

Blank bath	H2SO4 (M)	NaCl (M)	Na3Cit (M)	Dissolved metals; role in plating
Common blank	.00018	.1	.07	Fe, Mo; plating mix-in
High-H_2SO_4	1	0	.07	Co
High-H_2SO_4-Cl^-	1	1	0	Ni
No-Cl^-	.00018	0	.07	Cu
High-Cit^{3-}	.00018	.1	1	None; plating mix-in
High-Cl^-	.00018	1	.07	None; plating mix-in

Five identical trials of parallel dissolution of all five metals were performed; the final solutions for each separate metal were accumulated across all trials. Concentration tracking for one representative trial is plotted in Fig. 3(b). The dissolution of Fe, Cu, and Mo finished relatively early within several minutes; Co within a half-hour, and Ni slightly over one hour. The relative slopes indicate Ni and Cu dissolve at the fastest rate; followed by Fe, Co, and Mo.

The resulting separate-metal baths were then mixed with an additional blank bath component to create seven different plating

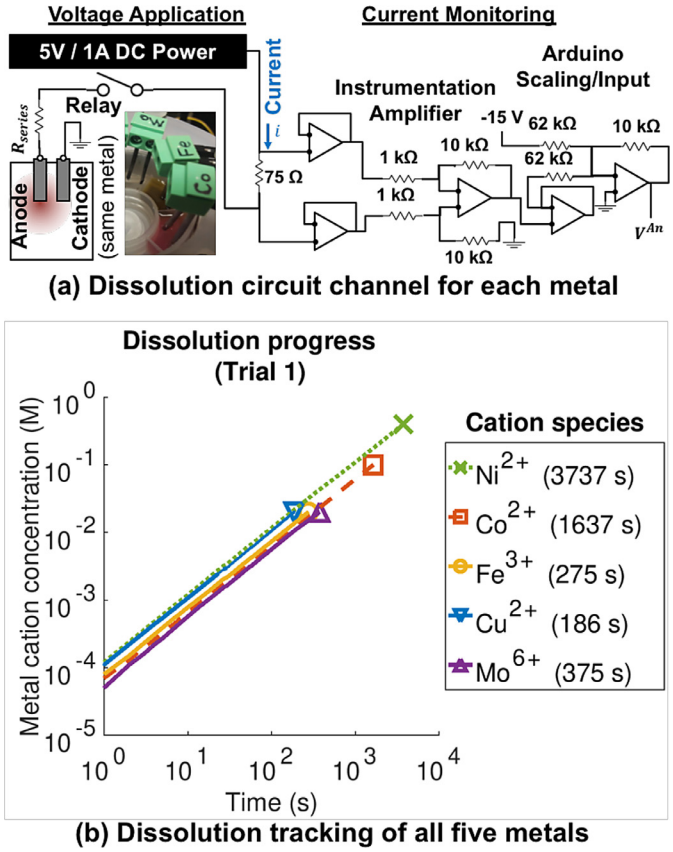

Fig. 3. Dissolution: (a) circuit channel for each metal, (b) process monitoring of concentration increase for all five metals.

baths with variations in supporting bath and metal cation concentrations. The default mixture across the separate plating baths (except for a few deliberate variations) included: .5 mL of the Ni, Co, Fe baths; .25 mL of the Cu and Mo baths; and .5 mL of a blank mix-in bath. Concentration variations across different species included those of acid (baths 1-3), supporting anion species (baths 4-5), and metal cations (baths 6-7). An overview of the plating baths is listed in Table 2, which made use of some of the blank baths detailed in Table 1.

To perform deposition, each mixed plating bath was transferred into the central chamber shown in Fig. 2(b), and a PtIr micro-tool was positioned into the tank using a Zaber LSA-10A micro stepper motor controlled by an Adafruit v2 Motorshield. Pillars were deposited in a voxel-by-voxel manner using closed-loop current

Table 2
Mixed plating baths for deposition.

Bath # and name	Blank mix-in	Exceptions from default
(1) low-acid	.5 mL common blank	None
(2) medium-acid	.25 mL CB .25 mL high-acid	None
(3) high-acid	.5 mL high-acid	None
(4) high-citrate	.25 mL CB .25 mL high-citrate	None
(5) high-chloride	.25 mL CB .25 mL high-chloride	None
(6) low-Co	.5 mL CB .25 mL high-acid	.25 mL Co bath .75 mL blank mix-in
(7) high-Mo	.25 mL CB .2s5 mL high-acid	.05 M dissolved Mo bath

monitoring and spike feedback, resembling that of prior work [12]. Each pillar consisted of 300 voxels with a vertical spacing of 4.5 μm. The deposition cell and custom electrochemical circuitry are shown in Fig. 4(a). The current and build times per voxel were monitored in-process, and an average was computed across all voxels for each run. Pillar shape and composition across bottom, middle, and top was characterized using SEM and EDX.; average values for the whole pillar were also computed. These values and averages are superimposed on the SEM images for each trial in Fig. 4(b-h).

Initially, the influence of the acid concentration was analyzed across baths 1-3. A medium-acid pillar width of 160 μm increased to 360 μm using the low-acid bath and decreased to 70 μm with

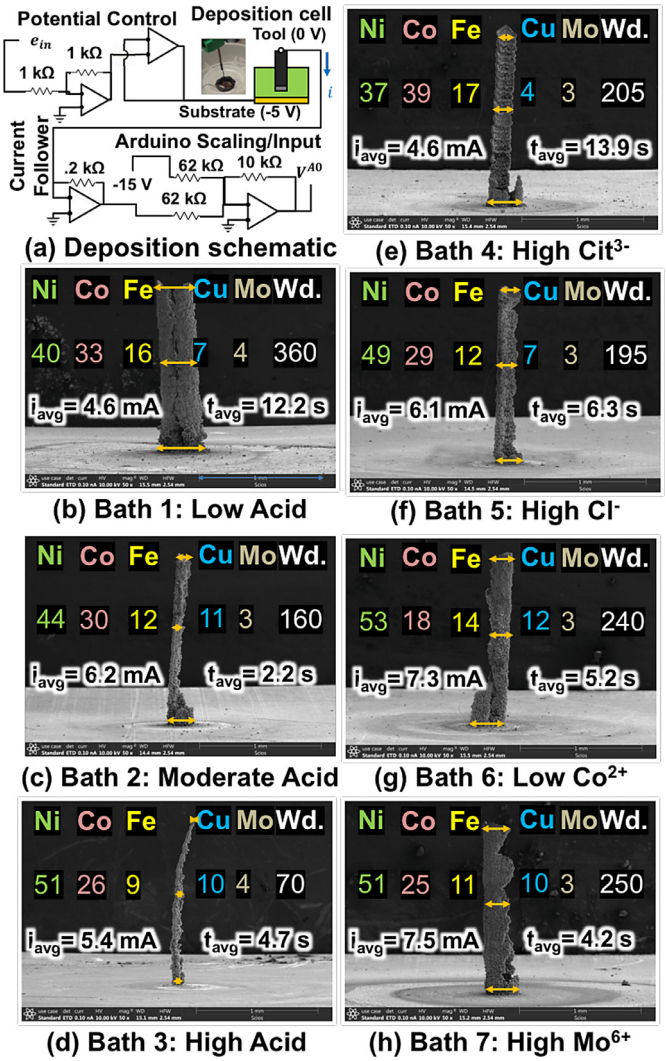

Fig. 4. Deposition: (a) setup, (b-h) results, including average atomic percentages of each metal; iavg denotes average current; tavg denotes average voxel build time; Wd.: avergage pillar width (μm).

increasing acid concentration. A slightly higher amount of iron-group metals (89%) were deposited in the low-acid condition compared to medium- and high-acid (86%). The moderate acid run had the highest current (6.2 mA) and shortest voxel build time (2.2 s), implying the fastest efficiency of deposition. Lower current magnitudes and longer build times were exhibited in the runs with low-acid (4.6 mA, 12.2 s) and high-acid (5.4 mA, 4.7 s). The moderate acid concentration was maintained in baths 4-7 for the subsequent study of anion and cation concentration influences. Next, the influence of anion species was examined. Relative to the reference moderate acid run (bath 2), use of increased citrate (bath 4) resulted in a slightly wider pillar (205 μm) with a higher amount of iron-group metals (93%), lower current (4.6 mA), and longer average voxel build time (13.9 s), resembling the effects of low acid. This may be due to the complexing effects of citrate inhibiting deposition in a similar manner to the reduced bath conductivity resulting from less acid. A higher chloride concentration enhanced the deposition of nickel (49%) compared to the reference (44%) and appeared to suppress deposition of the copper (7%) compared to the reference (11%), reflecting some of the influences mentioned in the literature review. However, the increase of this anion did not accelerate the overall run – the current decreased slightly (6.1 mA) and the average voxel build time increased nearly threefold (6.3 s) with respect to the reference run.

Finally, select metal cation concentrations were varied. Lower cobalt concentration yielded lower cobalt content (18%) compared to the reference (30%) as expected; and longer voxel time (5.2 S), likely due to fewer cations present for deposition; and an increased current magnitude (7.3 mA), possibly due to increased hydrogen evolution in the absence of metal ions available to deposit. An increase in aqueous Mo concentration did not increase the average percentage of Mo in the deposit compared to the reference (both 3%); increased the current magnitude (7.5 mA) and the build time (4.2 s), despite more ions in solution, suggesting a complexation mechanism inhibiting deposition.

An overall trend of lower deposition current accompanying a faster deposition rate was seen (except for few runs) – this was deemed a high current efficiency for deposition. The moderate acid reference bath yielded the fastest voxel build time at a relatively low current magnitude. Overall composition trends were also seen: baths 1,4, and 5 exhibited pillars with higher concentrations of Co and Fe; baths 2, 3, 6, and 7 yielded pillars with higher contents of Ni and Cu. The former pair have been reported to yield higher magnetic coercivity, and the latter to reduce coercivity [16], making the pairs suitable for fabricating hard versus soft magnetic materials respectively. For the latter pair, increased conductivity is associated with a higher Cu content [17]. Mo content remained relatively low – within 5% – across all baths and varied the least in response to all changes, even with an increase in aqueous concentration in trial 7. For pillar width, it was seen that acid was the most influential, causing a decrease in width with an increase in concentration. Less-significant fluctuations were seen in the remaining runs.

Overall, conditions for individual dissolution of each metal were established, along with the ability to mix separate dissolution baths into a combined plating bath. Influences of individual species variations upon mixing were observed.

3. Compositional grading

Up to this point, a suitable range of electrochemical conditions was identified to achieve separate-metal dissolution and deposition out of the manually-mixed separate dissolved baths. These initial findings allowed for an intermediate electrolytic bath to be identified out of which all processes for all five metals in the NiCoFeCuMo system could be executed in a single cell; consisting of.485 M H_3BO_3, .5 M Na_3Cit, .25 M H_2SO_4, and .5 M NaCl. All reactions occurred without major complications (some chloride film appeared on the copper electrode during dissolution, but did not impede the process and receded upon electrode deactivation). This allowed for the combined dissolution-deposition operation of ECAM in a fully-automated manner, as required in a production environment. In the combined cell, anodic dissolution of each metal was introduced at separate 1/5th intervals

throughout the pillar build, resulting in a dynamically-changing solution to yield compositional grading of the deposit. Pillars of 300 voxels spaced by 4.5 μm each were fabricated as before. The combined cell and dissolution-deposition sequence are illustrated in Fig. 5(a). Two concentration sequences were tested, shown in Fig. 5(b). Both contained .5 M of least-preferential Ni and .025 M of induced co-depositing Mo. Sequence (i) contained lower levels of the more-preferential Co, Fe, and Cu (.05 M, .02 M, and .005 M); (ii) contained higher levels (.1 M, .05 M, and .01 M). The compositional grading was evaluated across each 1/5th segment of the pillars. It was expected that the relative maximum percentage of each metal would be present within the segment built immediately after its dissolution; due to: (a) the depletion of each metal after its corresponding segment was built, (b) an expected lower degree of auxiliary plating on any preceding segments, and (c) the introduction of more-preferable metals in later segments.

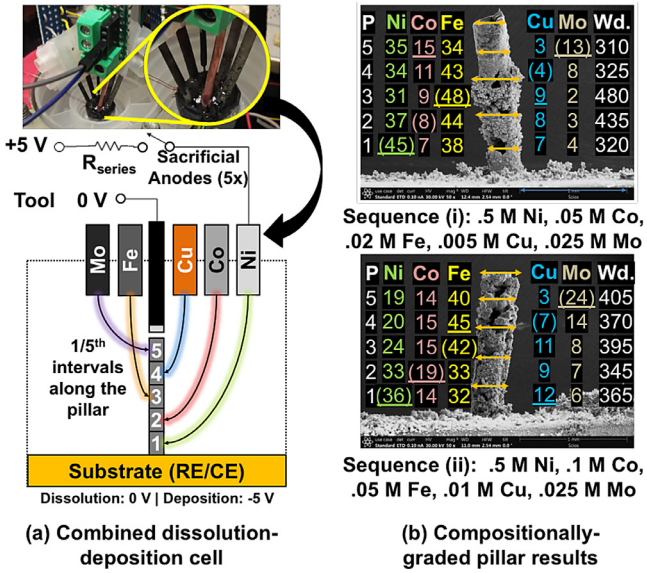

Fig. 5. Combined dissolution-deposition: (a) setup, (b) SEM and EDX results for 1/5th segments, where # indicates resultant maximum content; (#) indicates intended maximum content.

In both trials, segments containing Ni and Mo maxima matched the intended ones. Ni content was lower throughout the pillar in Trial 2 (19-36%), compared to Trial 1 (35-45%), reflecting the elevated concentrations of more-preferential Co, Fe, and Cu. Trial 2 yielded higher Mo content (6-24%) than in Trial 1 (2-13%), likely due to more iron-group species present to induce its co-deposition.

The Co and Fe grading patterns varied across the sequences. In (i), the intended and experimental Fe maxima matched (48% at segment #3); the Co maximum did not match. In (ii), the maxima of Co matched (19% at segment #2), but those of Fe did not. These behaviors suggest that both relatively-higher Co and relatively-lower Fe concentrations lead to more-controllable compositional grading patterns, reflecting the relative anomalous preferences.

The grading pattern of Cu deposition was the most irregular; the segments of maximum content of each failed to match the intended ones, instead of appearing in segments below the intended one. This is likely due to Cu being the most preferential and noble species of the system, resulting in increased deposition throughout the entire process and the lowest degree of control.

The second segment of the Trial 2 pillar met the definition of a high-entropy alloy, in which all metals were present in the 5-35% range. The remaining segments met most of the HEA criteria with a few exceptions – either below 5% content of Cu or Mo, or above 35% of Ni or Fe.

4. Conclusions and future work

This study demonstrated the electrochemical additive manufacturing of compositionally-graded NiCoFeCuMo parts using combined dissolution and deposition. The necessary electrolyte formulations to perform all operations were identified. The influences of varied supporting bath concentrations on the output deposition were studied; these were found to affect the pillar geometry and composition, with acid concentration yielding the most influence. Metal ion concentrations were varied during both manual mixing and combined dissolution-deposition; additionally, influencing the output pillar composition. Compositional grading of the pillar by anodic dissolution at discrete pillar segments was explored. The contents of Ni and Mo contents were most consistently controlled, followed by Co and Fe across different concentrations; Cu was the least-controllable. The atomic percentages neared the definition of a HEA in most regions and matched it in one region. This study serves as a fundamental proof-of-concept of electrochemical additive manufacturing of 5-metal NiCoFeCuMo HEA components, opening the door to further research studies in uniformity, repeatability, microstructure, properties, and larger sizes in part fabrication.

Declaration of Competing Interest

The authors declare that they have no known competing financial interests or personal relationships that could have appeared to influence the work reported in this paper.

Acknowledgments

This work was supported by the National Science Foundation under grants CMMI-1454181 and CMMI-1955842. Any opinions, findings, and conclusions, or recommendations expressed in this material are those of the author(s) and do not necessarily reflect the views of the National Science Foundation.

References

[1] Yeh JW, Chen SK, Lin SJ, Gan JY, Chin TS, Shun TT, et al. (2004) Nanostructured high-entropy alloys with multiple principal elements: novel alloy design concepts and outcomes. *Advanced Engineering Materials* 6:299–303.
[2] Sonkusare R, Yadav S, Gurao N, Biswas K (2020) High Entropy Alloys in Bulk Form: Processing Challenges and Possible Remedies. *High Entropy Alloys*, CRC Press. 125.
[3] Huser G, Demirci I, Aubry P, Guillot I, Perrière L, Rigal E, et al. (2020) Study of the elaboration of high entropy material from powder by laser additive manufacturing. *Procedia CIRP* 94:270-5.
[4] Schmidt M, Merklein M, Bourell D, Dimitrov D, Hausotte T, Wegener K, et al. (2017) Laser based additive manufacturing in industry and academia. *CIRP Annals* 66:561-83.
[5] Torralba JM, Campos M (2020) High entropy alloys manufactured by additive manufacturing. *Metals* 10:639.
[6] Bourell D, Kruth JP, Leu M, Levy G, Rosen D, Beese AM, et al. (2017) Materials for additive manufacturing. *CIRP annals* 66:659-81.
[7] Wits WW, Amsterdam E (2021) Graded structures by multi-material mixing in laser powder bed fusion. *CIRP Annals*.
[8] Efthymiou K, Pagoropoulos A, Papakostas N, Mourtzis D, Chryssolouris G (2014) Manufacturing systems complexity: An assessment of manufacturing performance indicators unpredictability. *CIRP Journal of Manufacturing Science and Technology* 7:324-34.
[9] Sundaram MM, Kamaraj AB, Kumar VS (2015) Mask-less electrochemical additive manufacturing: a feasibility study. *ASME Journal of Manufacturing Science and Engineering* : 137.
[10] Davydov A, Volgin V (2020) Electrochemical local maskless micro/nanoscale deposition, dissolution, and oxidation of metals and semiconductors (a review). *Russian Journal of Electrochemistry* 56:52-81.
[11] Sundaram M, Kamaraj AB, Lillie G (2018) Experimental study of localized electrochemical deposition of Ni-Cu alloy using a moving anode. *Procedia CIRP* 68:227-31.
[12] Brant A, Sundaram M (2021) Electrochemical additive manufacturing of graded NiCoFeCu structures for electromagnetic applications. *SME Manufacturing Letters*
[13] Kamaraj A, Lewis S, Sundaram M (2016) Numerical study of localized electrochemical deposition for micro electrochemical additive manufacturing. *Procedia CIRP* 42:788-92.
[14] Soni VK, Sanyal S, Sinha SK (2020) Phase evolution and mechanical properties of novel FeCoNiCuMox high entropy alloys. *Vacuum* 174:109173.
[15] Brenner A (1963) *Electrodeposition of alloys: principles and practice*, Academic Press.
[16] Mehrizi S, Sohi MH, Ebrahimi SS (2011) Study of microstructure and magnetic properties of electrodeposited nanocrystalline CoFeNiCu thin films. *Surface and Coatings Technology* 205:4757-63.
[17] Loboda V, Khursenko S (2006) Structure and electrical conductivity of ultrathin Ni-Cu films. *Journal of Experimental and Theoretical Physics* 103:790-4.